The International Archives of the Photogrammetry, Remote Sensing and Spatial Information Sciences, Volume XLIX-B3-2026
XXV ISPRS Congress 2026 "From Imagery to Understanding", Commission III, 4–11 July 2026, Toronto, Canada

Casting a Neural Net: Satellite-based Coastline Extraction with Neural Networks across Diverse Coastal Environments in British Columbia, Canada

Piper Steffen [a, *], Mohsen Ghanbari [a], Maycira Costa [a]

[a] Spectral Remote Sensing Laboratory, Dept. of Geography, University of Victoria, Victoria, BC V8P 5C2, Canada
[*] pipersteffen@uvic.ca

Keywords: Coastline extraction, Satellite-derived shoreline, Coastal monitoring, Sentinel-2, Machine Learning, British Columbia.

Abstract

As climate change is increasingly affecting marine and terrestrial ecosystems, researchers, resource managers, and coastal communities are using satellite-based remote sensing, such as Sentinel-2 multispectral imagery, to monitor coastal environments at large scales. The ability to automatically define the position of the coastline from imagery, referred to as "coastline extraction", is a valuable tool in extending monitoring of coastal ecosystems, such as kelp forests and eelgrass meadows, to regional and provincial scales. In this work, we present a new dataset for water segmentation, and thus coastline extraction, consisting of manually annotated Sentinel-2 images acquired at low tide, specific to the Pacific coast of British Columbia (BC), Canada. We then evaluate three methods for coastline extraction: an adaptive thresholding method, and two convolutional neural networks trained on firstly, a global dataset and secondly, our newly created BC dataset. The model trained on the BC dataset achieved the highest accuracy across standard image segmentation metrics and in coastline positional error measured relative to a manually defined reference coastline. Additionally, very-high resolution unmanned aerial vehicle data collected at validation sites with comparable tide levels to the Sentinel-2 dataset imagery showed that training on BC specific data decreases pixel misclassification, and therefore coastline positional error, due to the presence of subtidal and intertidal algae and vegetation at various validation sites in the study area.

1. Introduction

Within British Columbia (BC), Canada, over 64% of the population lives within 10 kilometres of the Pacific Ocean, where coastal economies, valued at over $21 billon, are closely tied to the health of marine ecosystems (Government of British Columbia, 2024). Ecologically, coastal ecosystems provide critical habitat and forage opportunities for important species, including salmon and Pacific herring (Government of British Columbia, 2024). As these ecosystems are increasingly affected by climate change and anthropogenic stressors, various levels of governance in BC have prioritized monitoring of coastal ecosystems, such as canopy-forming kelp forests (Government of British Columbia, 2024). Multiple studies have documented loss, change, and resilience of kelp forests throughout BC by analysing satellite imagery of the coastal zone (Gendall et al., 2023; Man et al., 2025; Mora-Soto et al., 2024; Nijland et al., 2019; Wachmann et al., 2026). In this context, a precise delineation of the coastline, defined as the physical boundary between water and land (Boak & Turner, 2005), particularly at low tide, can significantly improve the accuracy of kelp detection algorithms by masking land and intertidal areas that may introduce false positives (Cavanaugh et al., 2021; Gendall et al., 2023).

The most rudimentary approach to coastline extraction involves manual delineation through visual interpretation of imagery. However, this process is time-consuming and costly (Boak & Turner, 2005), limiting its feasibility to large scales, such as BC's over 26,000 kilometres of coastline (Government of British Columbia, 2024). Automated methods for coastline extraction provide a promising, scalable alternative to this with the availability of medium-resolution satellite imagery, including Landsat and Sentinel-2 (McAllister et al., 2022). Broadly, the process for satellite-based coastline extraction is comprised of two steps: 1) image segmentation, where the input imagery is classified per-pixel (i.e. segmented) as water or non-water to produce a binary mask of predicted class, and 2) vectorization of the boundary between water and non-water classes to define coastline position.

For image segmentation, many water indices have been developed such that a predefined threshold value divides water and non-water pixels (Feyisa et al., 2014; McFeeters, 1996; Rad et al., 2021; Xu, 2006). However, adaptive thresholding algorithms provide a more robust method for determining an optimal threshold value that accounts for varying image illumination conditions (Pucino et al., 2022). The most common is Otsu's method, which defines a threshold value based on an image's pixel intensity distribution to minimize intra-class variance, in this case for water and non-water classes (McAllister et al., 2022; Otsu, 1979). Alternatively, water indices may be used alongside spectral bands as input to a wide range of machine learning (ML) algorithms that perform image segmentation without determining a threshold value (Pucino et al., 2022; Seale et al., 2022; Vos, Harley, et al., 2019; Yang et al., 2020). One key advantage of these algorithms, particularly deep learning algorithms such as convolutional neural networks (CNNs), is that the spatial arrangement of pixels is considered during segmentation, rather than pixel intensity values alone as in threshold-based methods (McAllister et al., 2022). ML-based methods for coastal image segmentation have demonstrated high performance, although critically, have been primarily evaluated along smooth sand beaches (Bishop-Taylor et al., 2021; Pucino et al., 2022; Vos, Harley, et al., 2019). Further, multiple studies have found that images acquired during low tide result in lower accuracy compared to images acquired during high tide, due to the added complexity of the intertidal zone (Pucino et al., 2022; Seale et al., 2022; Vos, Harley, et al., 2019). This is particularly relevant in coastal BC, where rocky, heterogeneous intertidal zones are common and smooth sand beaches are relatively rare (ShoreZone, 2025), presenting an additional challenge to local coastline extraction.

Here, we evaluate three methods of coastline extraction, including a threshold-based method and two ML methods using CNNs, applied to medium-resolution (10 m) Sentinel-2 imagery of BC acquired during low tide. As a pilot study, we select 8 geomorphologically complex validation sites in the Broughton Archipelago, northeast of Vancouver Island, and consider very-high resolution unmanned aerial vehicle (UAV) imagery acquired during comparable tide level and time of year to inform understanding of site-specific ground truth conditions. Existing data products for the low water line published by the Government of British Columbia are known to be unreliable, with numerous examples of obvious errors (GeoBC Branch, 2013). Thus, a comprehensive method for coastline extraction from Sentinel-2 imagery acquired at low tide in BC provides a key method for further research into the impact of climate change on coastal ecosystems.

2. Methods

2.1 Study Area

The Pacific coast of BC is characterized by a heterogeneous mix of coastal features, formed over multiple periods of glaciation that eroded steep fjords and valleys interspersed with nutrient-rich deltas and inclined pebble and sediment beaches formed by centuries of river and ocean currents (ShoreZone, 2025; Thomson, 1981). As part of the Northern Shelf biogeographical region, the Broughton Archipelago (Figure 1), the traditional territories of the 'Na̱mgis, Mamalilikulla, and Kwikwasut'inuxw First Nations, located northeast of Vancouver Island, was selected as a study area to represent the complexity of the BC coastline. Tides in the region are mesotidal, with a mean tidal range of 3.4 m (Fisheries and Oceans Canada, 2026). Canopy-forming kelp forests are common along moderately inclined rocky substrate (Man et al., 2025), while subtidal and intertidal eelgrass meadows form along flat, sandy coastlines (ShoreZone, 2025). The complex terrestrial and intertidal terrain, either steep or with a wide intertidal zone including algae and vegetation, provides additional complexity to the coastline extraction task as the boundary between water and land may be difficult to discern due to shadows, pixel mixing, and adjacency effects (Bishop-Taylor et al., 2021; Seale et al., 2022).

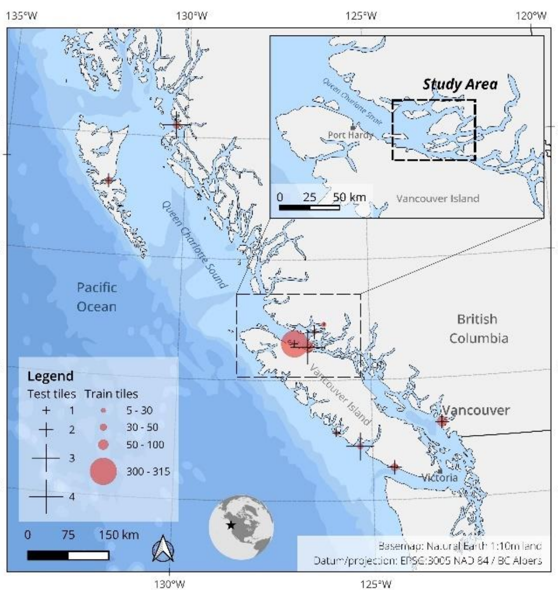

Figure 1: Map of coastal British Columbia, Canada, showing location of study area (inset) and distribution of BC dataset image tiles.

Coastline extraction methodologies are evaluated at 8 validation sites within the study area. Sites were selected to encompass a range of coastal geomorphology and vegetation conditions present in BC, including sand and pebble beaches, small river estuaries, rock platforms, steep foreshore slopes, dense intertidal eelgrass, and dense subtidal canopy-forming kelps.

2.2 Methodology

In this work we evaluate 3 methods of coastline extraction: 1) a threshold-based model using Otsu's method and a single water index, 2) a CNN trained on an existing global dataset, and 3) a CNN trained on a newly created BC dataset of curated Sentinel-2 images. In-situ UAV data provides insight into method performance across diverse coastal environments. Our approach follows four broad steps illustrated in Figure 2: 1) image selection and data annotation to create a new BC dataset for CNN training and evaluation, 2) model training, 3) image segmentation, and 4) vectorization to delineate coastline position. Each method is assessed by measuring image segmentation performance and coastline positional accuracy relative to a reference coastline.

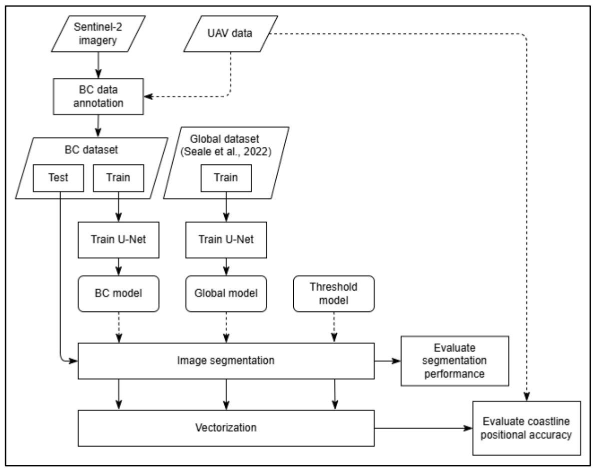

Figure 2: Methodology flowchart including datasets, processing, and evaluation methods.

2.2.1 UAV Data: Georeferenced true-colour UAV imagery (3-5 cm spatial resolution) is used to assist with data annotation and visualization of relevant coastal geomorphological and biological factors during model evaluation, such as substrate material, intertidal features (i.e. large rocks or vegetation that may cast shadows), and presence of subtidal and intertidal algae and vegetation. UAV imagery was acquired at validation sites during periods of low tide in June 2025 in collaboration with the 'Na̱mgis First Nation and with permission of the Mamalilikulla and Kwikwasut'inuxw First Nations. The tide level at each site at the time of image acquisition was estimated relative to mean sea level (MSL) using the FES2022 global tide model (LEGOS et al., 2024).

2.2.2 Global Dataset: The Sentinel-2 Water Edges Dataset (SWED) is a globally distributed dataset consisting of Sentinel-2 images and labelled masks identifying water and non-water pixels (Seale et al., 2022). Image tiles and labels (256 x 256 pixels) are pre-allocated into train and test sets for robust algorithm benchmarking, with test tiles equally divided between source images acquired at high and low tides (Seale et al., 2022). Despite near global coverage, SWED does not include any tiles along the Northern Pacific coast of North America, with the nearest test tiles located in Western Alaska, USA and Baja, Mexico. Hereafter, this is referred to as the "global dataset".

2.2.3 BC Dataset: In this work, we introduce a newly constructed Sentinel-2 water segmentation dataset, following the structure of SWED, specific to coastal BC and low tide images. The dataset contains 713 tiles (256 x 256 pixels) extracted from 8 Sentinel-2 Level-2A images (bottom-of-atmosphere reflectance) acquired during low tide (< 1.4 m relative to MSL) and distributed throughout the southern and northern BC coast, separated into train (n=692) and test (n=21) splits (Figure 1). Where UAV data was available, Sentinel-2 images were selected such that the tide level at each validation site is comparable to the corresponding UAV image, within 0.3 m absolute difference.

Tile labels defining water (1) and non-water (0) pixels were created by expert image interpretation and manual vector annotation using QGIS software (QGIS Development Team, 2023), considering the true-colour composite, false colour infrared composite (NIR-R-G), and two water indices as greyscale: NDWI (McFeeters, 1996) and MNDWI (Xu, 2006). Data annotation was done by a trained remote sensing analyst and validated for a random sample of tiles by comparing to a second analyst's independent annotation of the same data, with minimal differences. At sites where UAV data was available, it was consulted to provide additional environmental context. Otherwise, high-resolution base maps (ESRI Satellite, Google Satellite) were considered, however varying tide levels and time of year limit direct comparison with dataset imagery. Finally, vector annotations were rasterized in QGIS, and tiles were exported with 50% overlap of adjacent tiles to maximize data availability. Additionally, training tiles were restricted to have zero spatial overlap with test tiles. The resulting image and label tiles, pre-allocated into train and test splits, form what is hereafter referred to as the “BC dataset”.

2.2.4 Image Segmentation: The 3 coastline extraction methods evaluated in this work use 3 unique models for image segmentation: a simple threshold-based model applying Otsu's method to a single water index, a CNN model trained on the global dataset (SWED), and a second CNN model trained on the BC dataset.

For the threshold model, 5 water indices calculated from the visible, near-infrared, and shortwave infrared Sentinel-2 spectral bands were considered: the Normalized Difference Water Index (NDWI) (McFeeters, 1996), Modified Normalized Difference Water Index (MNDWI) (Xu, 2006), Augmented Normalized Difference Water Index (ANDWI) (Rad et al., 2021), and Automated Water Extraction Index, with and without shadows ($AWEI_{sh}$ and $AWEI_{nsh}$) (Feyisa et al., 2014). Preliminary assessment of Otsu's thresholding applied to NDWI, MNDWI, ANDWI, $AWEI_{sh}$, and $AWEI_{nsh}$ indicated that $AWEI_{sh}$ demonstrated the best performance in BC coastal regions, thus forming what is hereafter referred to as the threshold model.

For the ML methods, two CNNs with U-Net architecture (Ronneberger et al., 2015) were trained using the Python Segmentation Models PyTorch library (Iakubovskii, 2019) for implementation. Hereafter, “global model” refers to the CNN trained on the global dataset, whereas “BC model” refers to the CNN trained on the BC dataset. Training data input to both models was composed of image tiles including 7 spectral bands (at or resampled to 10 m spatial resolution) and 5 water indices: red, green, blue, near-infrared (NIR), 2 shortwave infrared bands (SWIR1, SWIR2), NDWI, MNDWI, ANDWI, $AWEI_{sh}$, and $AWEI_{nsh}$. The global dataset provides image tiles after resampling the 20 m SWIR bands using nearest neighbour interpolation (Seale et al., 2022), whereas in the BC dataset SWIR bands were resampled using bilinear interpolation, which provided smoother greyscale water indices. During CNN model training, each model iteratively “learns” to classify water and non-water pixels based on the input image tiles and associated labels to produce a predicted binary classification mask as output.

2.2.5 Vectorization: Following image segmentation, a subpixel resolution contour algorithm, specifically marching squares with linear interpolation (Cipolletti et al., 2012), is applied to the boundary between water and non-water classes in the segmentation output to delineate the modelled coastline position. Vectorization is applied to the outputs of the threshold, global, and BC segmentation models and defines the coastlines referred to hereafter as the threshold, global, and BC model coastlines, respectively. Further, tile labels from the BC dataset (annotation masks defining water and non-water pixels) covering the 8 validation sites are processed equivalently, applying the same contour algorithm to the boundary between classes, to produce a reference coastline with which to evaluate the threshold, global, and BC model coastline's positional accuracy.

2.2.6 Model Evaluation: Each coastline extraction model is evaluated in two ways: first, image segmentation performance is measured using the BC test dataset, and second, coastline positional accuracy is assessed qualitatively and quantitatively across 8 validation sites. Image segmentation performance is determined by calculating 5 standard segmentation metrics: accuracy, precision, recall, F1-score, and intersection over union (IOU). Coastline positional accuracy is assessed by calculating the minimum distance between the model coastline and reference coastline. Points are distributed along the model coastline at 5 m intervals, at which error is calculated as the distance from the model-derived coastline to the nearest point along the reference coastline (Figure 3). A positive error value (i.e. the model coastline is offset from the reference on the water side) indicates a seaward bias, while a negative error value indicates a landward bias.

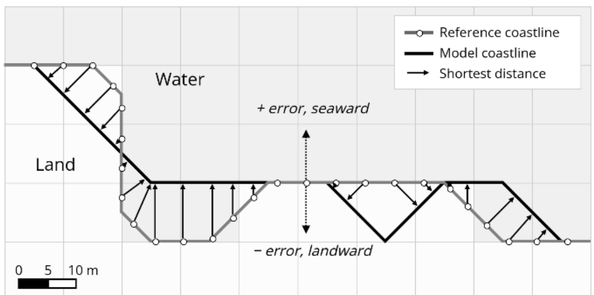

Figure 3: Illustration of methodology used to assess coastline positional accuracy.

3. Results

3.1 Image Segmentation Performance

Except recall, the BC model outperformed the threshold and global models across all image segmentation performance metrics (Table 2). In this case, true positive (TP) pixels are those correctly identified as water, true negatives (TN) are those correctly identified as non-water, and false positives (FP) and false negatives (FN) are those incorrectly identified as water and non-water, respectively. The BC model exhibits higher precision than the threshold and global models, indicating a lower false positive rate (non-water pixels misclassified as water). In contrast, the threshold model results in a marginally higher recall than the BC model, indicating a slightly lower false negative rate (water pixels misclassified as non-water). Notably, the BC model has a higher accuracy, F1-score, and IOU than the threshold (1.3%, 0.9%, 1.8% increase) and global (3.3%, 4.0%, and 7.8% increase) models.

	Formula	Threshold model	Global model	BC model
Accuracy	$\frac{TP+TN}{TP+TN+FP+FN}$	0.979	0.960	**0.992**
Precision	$\frac{TP}{TP+FP}$	0.973	0.921	**0.990**
Recall	$\frac{TP}{TP+FN}$	**0.992**	0.988	0.991
F1-score	$2 \cdot \frac{precision \cdot recall}{precision + recall}$	0.982	0.953	**0.991**
IOU	$\frac{TP}{TP+FP+FN}$	0.965	0.911	**0.982**

Table 2: Image segmentation performance metrics, formula, and results, for the threshold, global, and BC models. The highest value is bolded for each metric.

3.2 Coastline Positional Accuracy

Across 8 validation sites, the BC model coastline achieved a mean error (ME) of −0.96 m (seaward) and a mean absolute error (MAE) of 3.66 m, the lowest of all models (Table 3). The highest errors were observed for the global model coastline with a ME of −3.37 m (seaward) and a MAE of 11.64 m, followed by the threshold model coastline with a ME of +3.08 m (landward) and a MAE of 9.87 m. Based on the error distributions shown in Figure 4, the BC model shows the lowest error range, with values most concentrated around zero, whereas the global and threshold models have a greater range. Notably, the threshold model shows a predominant positive error bias (landward), while the global model shows a similar but opposite negative error bias (seaward). This is corroborated by the differing signs of the ME values for each model. Results of a Kruskal-Wallis test (Kruskal & Wallis, 1952) for statistical significance of the coastline positional error distributions indicate a significant difference in at least one of the models ($p < 0.001$). Further, post-hoc Dunn's tests (Dunn, 1964) with Bonferroni correction indicate significant P-values for each of the 3 pairwise comparisons ($p < 0.001$).

	Threshold model	Global model	BC model
ME	3.08 m	-3.37 m	**-0.96 m**
MAE	9.87 m	11.64 m	**3.66 m**

Table 3: Cumulative coastline positional error metrics for the threshold, global, and BC models relative to the reference coastline. ME = mean error; MAE = mean absolute error.

Examples of the strengths and weaknesses of the BC model in comparison to the threshold and global models in terms of coastline position are shown in Figure 5. Overall, the BC model most closely follows the reference coastline and has relatively lower outlier errors, generally within 10 m, corresponding to Sentinel-2 pixel resolution. Specifically, at site 1, a relatively smooth coastline with a high reflectance foreshore is most closely represented by the BC model. In contrast, the global model incorrectly identifies the foreshore vegetation line as coastline, or extends seaward beyond the middle section of mixed, intertidal pixels. The threshold model results in some improvements compared to the global model, but critically, includes numerous misclassified single pixels along the foreshore, leading to multiple short coastlines. At site 2, all three models exhibit higher performance, as indicated by the decreased magnitude of the y-axis, with the global and threshold models showing a consistent seaward bias in error. Site 3 includes a small estuary, where contrary to sites 1 and 2, the threshold model significantly underperforms the BC and global models by misidentifying the boundary between inland wet-sediment and vegetation as the coastline. However, similar to site 1, the threshold model produces multiple short, enclosed coastlines due to misclassified land pixels. Site 4 shows a small, curved bay with a moderately wide foreshore, where the global model tends to place the coastline seaward while the threshold model places it further inland. Although the global and threshold models demonstrate similar magnitudes of mean error, they differ in the overall direction of the errors.

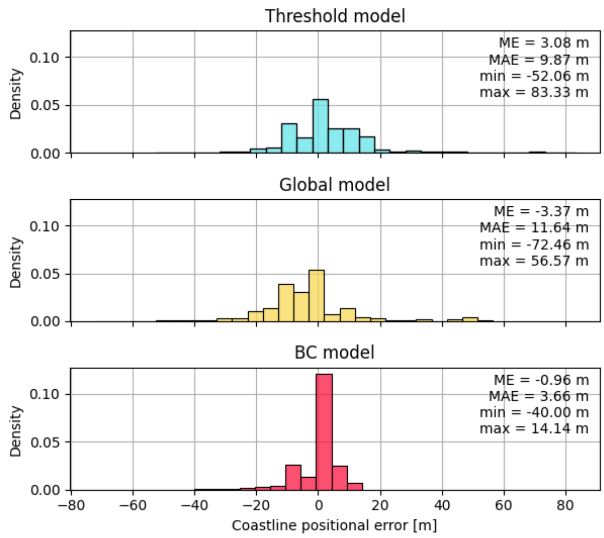

Figure 4: Coastline positional error distribution for the threshold, global, and BC models measured relative to the reference coastline across 8 validation sites.

4. Discussion

Results indicate that the BC model outperforms the global and threshold models in terms of image segmentation performance and coastline positional accuracy. The BC model achieved an IOU of 0.982, surpassing the performance of models developed in previous works (Pucino et al., 2022; Seale et al., 2022). We attribute this result to a few key differences between this and previous works: foremost, the BC dataset is predominantly located within the study area (Figure 1), likely contributing to spatial autocorrelation of the train and test datasets, which is known to inflate performance of segmentation model metrics (Kattenborn et al., 2022). Secondly, previous work by Seale et al. (2022) focused on developing a geographically generalizable model using a globally-distributed dataset, which, by nature of ML model training, comes at the expense of performance in individual locations (Seale et al., 2022; Wang et al., 2017). Although Pucino et al. (2022) developed a CNN for a constrained region of southern Australia, the model included imagery from a range of tidal states and degrees of coastal exposure, resulting in a model that outperformed Seale et al. (2022), and approached the IOU achieved in this work.

Beyond these methodological differences in model construction between past authors and this study, image segmentation performance metrics alone are not representative of a model's ability to accurately define coastline position. Since segmentation metrics are calculated from all pixels in a test dataset, values are heavily skewed by large regions of water and non-water that can be easily distinguished. Thus, a model's ability to classify pixels in the immediate vicinity of the coastline, where intertidal material, biological features, pixel mixing, and adjacency effects are most prevalent, is not adequately captured. Therefore, we consider segmentation metrics secondary to measuring coastline positional accuracy in assessing coastline extraction methodologies.

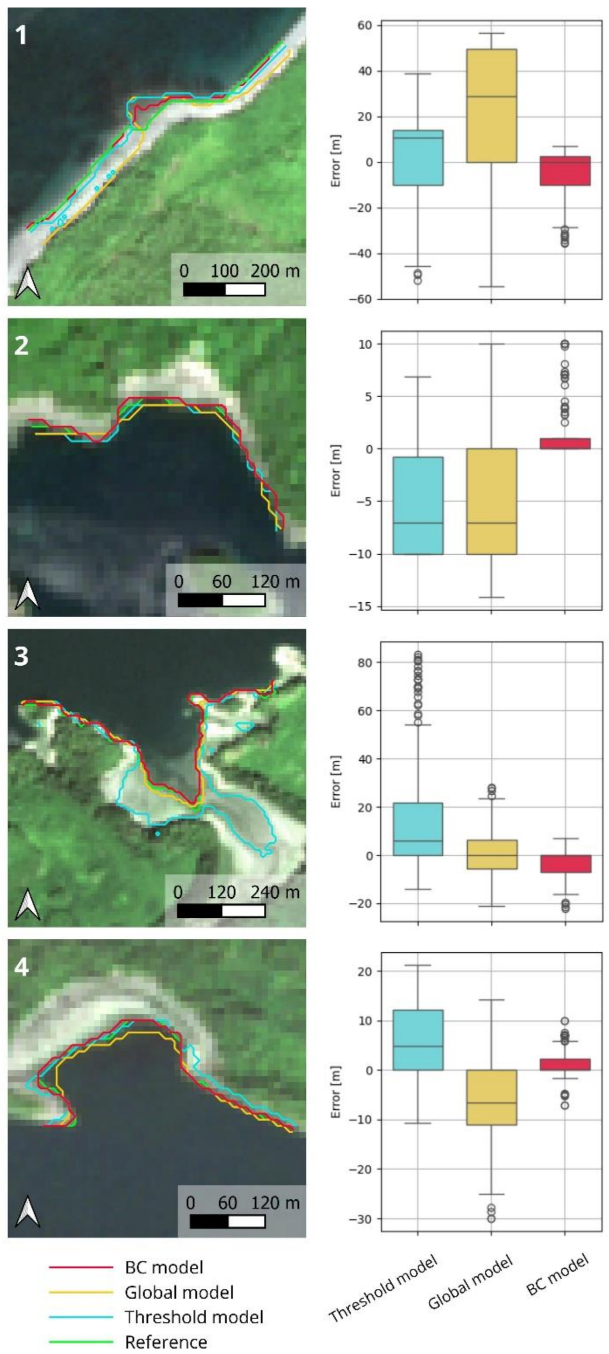

Figure 5: Comparison of the threshold, global, and BC model coastlines for 4 selected validation sites in the study area. Left: Sentinel-2 true color composite image with model-derived and reference coastlines overlayed. Image saturation is decreased for clarity. Right: boxplots of model coastline positional error relative to the reference coastline.

The BC model achieved a lower coastline positional ME (−0.96 m, seaward) and MAE (3.66 m) than the global and threshold models, with an overall seaward bias that is consistent with previous research (Hagenaars et al., 2018; Pucino et al., 2022; Vos, Harley, et al., 2019; Vos, Splinter, et al., 2019). Conversely, the threshold model produced a landward bias in ME, consistent with the previous evaluation of this combination of thresholding method and water index (Pucino et al., 2022). The BC model also achieved a lower ME and MAE than previous studies (Pucino et al., 2022; Vos et al., 2023; Vos, Harley, et al., 2019), yet the validity of this comparison is limited by differences in how coastline positional error is calculated. Typically, error is calculated along transects perpendicular to the coastline at known locations, but the high curvature of coastlines in BC made this method impractical for our study area.

Although the threshold model marginally outperforms the global model in terms of coastline positional accuracy, qualitative analysis of the extracted coastlines at the site level demonstrates significant disadvantages of the threshold model that are not captured by quantitative metrics alone, such as single-pixel misclassifications along the foreshore resulting in multiple, short coastlines. This supports previous observations on the evaluation of coastline extraction methods, which argue that qualitative analysis is required in addition to quantitative metrics to gain a robust understanding of methodology performance (Seale et al., 2022). Furthermore, qualitative assessment of site level results (Figure 5) shows that the ML-based models (the global and BC models) produce a smoother coastline vector that more consistently follows the shape of the reference coastline. This is attributed to how CNN models consider neighbouring pixels at various scales when classifying pixels as water or non-water. However, this also means that CNN models tend to struggle to identify small, linear, and narrow features in imagery, such as piers (Seale et al., 2022). This represents a key limitation of this work, as our validation sites do not include examples of anthropogenic coastal features such as ports, docks, and piers.

By comparing results with in-situ UAV imagery of validation sites, we can attribute common sources of coastline positional error due to geomorphological and biological factors. Very high-resolution imagery of sites 1, 2, and 4 (Figure 5) show the presence of intertidal algae and vegetation, most prominently eelgrass, in the immediate vicinity of the coastline. This may contribute to the global model’s misclassification of nearshore pixels in which algae and vegetation significantly contribute to pixel reflectance, leading to a seaward bias. This is somewhat mitigated by the BC model, thus suggesting that including training data representative of this scenario is critical to increasing performance in this region. Although the threshold model performs marginally better than the global model at these sites, it has another major disadvantage of misclassifying non-water pixels as water when wet sediment is predominant, demonstrated by site 3. To address this, further research is required to quantitatively determine how algae, vegetation, and substrate material may affect coastline positional error, thereby extending coastline extraction methodologies to the entirety of BC’s Pacific coast and beyond.

5. Conclusion

In this work, we introduce a new BC dataset for Sentinel-2 water/non-water image segmentation of low tide images and demonstrate its application to coastline extraction. The CNN model trained on the BC dataset outperforms the model trained on the global dataset and the threshold model employing Otsu’s method and $AWEI_{sh}$ in terms of image segmentation metrics and coastline positional accuracy, achieving mean and mean absolute errors of less than one Sentinel-2 pixel (10 m). The ability to define coastline position from Sentinel-2 images acquired during low tide is a valuable tool for coastal researchers and managers using medium-resolution satellite data to monitor coastal environments and understand how climate change impacts ecosystems at regional and local scales.

Acknowledgements

The authors acknowledge that this study was conducted on the traditional and unceded territories of the ’Na̲mgis, Mamalilikulla, and Kwikwasut’inuxw First Nations. Data collection was undertaken in collaboration with the ’Na̲mgis First Nation – special thanks to Nic, Danny, and Jack from ’Na̲mgis Natural Resources – and with permission of the Mamalilikulla and Kwikwasut’inuxw First Nations.

Funding for this work was provided by the Canadian Space Agency (CSA) [24AO3VIC33]. The FES2022 Tide product used in this work was funded by CNES, produced by LEGOS, NOVELTIS, and CLS, and made freely available by AVISO.

References

Bishop-Taylor, R., Nanson, R., Sagar, S., & Lymburner, L., 2021: Mapping Australia’s dynamic coastline at mean sea level using three decades of Landsat imagery. *Remote Sensing of Environment*, 267, 112734. doi.org/10.1016/j.rse.2021.112734.

Boak, E., & Turner, I., 2005: Shoreline Definition and Detection: A Review. *Journal of Coastal Research Journal of Coastal Research*, 21, 688–703. doi.org/10.2112/03-0071.1.

Cavanaugh, K. C., Bell, T., Costa, M., Eddy, N. E., Gendall, L., Gleason, M. G., Hessing-Lewis, M., Martone, R., McPherson, M., Pontier, O., Reshitnyk, L., Beas-Luna, R., Carr, M., Caselle, J. E., Cavanaugh, K. C., Flores Miller, R., Hamilton, S., Heady, W. N., Hirsh, H. K., … Schroeder, S. B., 2021: A Review of the Opportunities and Challenges for Using Remote Sensing for Management of Surface-Canopy Forming Kelps. *Frontiers in Marine Science*, 8. doi.org/10.3389/fmars.2021.753531.

Cipolletti, M. P., Delrieux, C. A., Perillo, G. M. E., & Cintia Piccolo, M., 2012: Superresolution border segmentation and measurement in remote sensing images. *Computers & Geosciences*, 40, 87–96. doi.org/10.1016/j.cageo.2011.07.015.

Dunn, O. J., 1964: Multiple Comparisons Using Rank Sums. *Technometrics*, 6(3), 241–252. doi.org/10.1080/00401706.1964.10490181.

Feyisa, G. L., Meilby, H., Fensholt, R., & Proud, S. R., 2014: Automated Water Extraction Index: A new technique for surface water mapping using Landsat imagery. *Remote Sensing of Environment*, 140, 23–35. doi.org/10.1016/j.rse.2013.08.029.

Fisheries and Oceans Canada, 2026. Tide and Current Tables: Volume 6. Canadian Hydrographic Service, Ottawa Ontario, Canada. waves-vagues.dfo-mpo.gc.ca/library-bibliotheque/chs-shc-tct-tmc-vol6-2026-41311267.pdf.

Gendall, L., Schroeder, S. B., Wills, P., Hessing-Lewis, M., & Costa, M., 2023: A Multi-Satellite Mapping Framework for Floating Kelp Forests. *Remote Sensing*, 15, 1276. doi.org/10.3390/rs15051276.

GeoBC Branch, 2013. CHS Low Water Mark Lines. GeoBC Branch, Victoria, British Columbia, Canada. catalogue.data.gov.bc.ca/dataset/chs-low-water-mark-lines (28 January 2025).

Government of British Columbia, 2024: B.C. Coastal Marine Strategy. www2.gov.bc.ca/gov/content/environment/air-land-water/water/bc-coastal-marine-strategy (17 November 2025).

Hagenaars, G., de Vries, S., Luijendijk, A. P., de Boer, W. P., & Reniers, A. J. H. M., 2018: On the accuracy of automated shoreline detection derived from satellite imagery: A case study of the sand motor mega-scale nourishment. *Coastal Engineering*, 133, 113–125. doi.org/10.1016/j.coastaleng.2017.12.011.

Iakubovskii, P., 2019. Segmentation Models Pytorch. GitHub. github.com/qubvel/segmentation_models.pytorch (12 March 2026).

Kattenborn, T., Schiefer, F., Frey, J., Feilhauer, H., Mahecha, M. D., & Dormann, C. F., 2022: Spatially autocorrelated training and validation samples inflate performance assessment of convolutional neural networks. *ISPRS Open Journal of Photogrammetry and Remote Sensing*, 5, 100018. doi.org/10.1016/j.ophoto.2022.100018.

Kruskal, W. H., & Wallis, W. A., 1952: Use of Ranks in One-Criterion Variance Analysis. *Journal of the American Statistical Association*, 47(260), 583–621. doi.org/10.1080/01621459.1952.10483441.

LEGOS, NOVELTIS, & CLS., 2024: FES2022 (Finite Element Solution) Ocean Tide. CNES. doi.org/10.24400/527896/A01-2024.004.

Man, L., Barbosa, R. V., Reshitnyk, L. Y., Gendall, L., Wachmann, A., Dedeluk, N., Kim, U., Neufeld, C. J., & Costa, M., 2025: Canopy-forming kelp forests persist in the dynamic subregion of the Broughton Archipelago, British Columbia, Canada. *Frontiers in Marine Science*, 12. doi.org/10.3389/fmars.2025.1537498.

McAllister, E., Payo, A., Novellino, A., Dolphin, T., & Medina-Lopez, E., 2022: Multispectral satellite imagery and machine learning for the extraction of shoreline indicators. *Coastal Engineering*, 174, 104102. doi.org/10.1016/j.coastaleng.2022.104102.

McFeeters, S. K., 1996: The use of the Normalized Difference Water Index (NDWI) in the delineation of open water features. *International Journal of Remote Sensing*. (world). doi.org/10.1080/01431169608948714.

Mora-Soto, A., Schroeder, S., Gendall, L., Wachmann, A., Narayan, G., Read, S., Pearsall, I., Rubidge, E., Lessard, J., Martell, K., & Costa, M., 2024: Back to the past: Long-term persistence of bull kelp forests in the Strait of Georgia, Salish Sea, Canada. *Frontiers in Marine Science*, 11. doi.org/10.3389/fmars.2024.1446380.

Nijland, W., Reshitnyk, L., & Rubidge, E., 2019: Satellite remote sensing of canopy-forming kelp on a complex coastline: A novel procedure using the Landsat image archive. *Remote Sensing of Environment*, 220, 41–50. doi.org/10.1016/j.rse.2018.10.032.

Otsu, N., 1979: A Threshold Selection Method from Gray-Level Histograms. *IEEE Transactions on Systems, Man, and Cybernetics*, 9(1), 62–66. IEEE Transactions on Systems, Man, and Cybernetics. doi.org/10.1109/TSMC.1979.4310076.

Pucino, N., Kennedy, D. M., Young, M., & Ierodiaconou, D., 2022: Assessing the accuracy of Sentinel-2 instantaneous subpixel shorelines using synchronous UAV ground truth surveys. *Remote Sensing of Environment*, 282, 113293. doi.org/10.1016/j.rse.2022.113293.

QGIS Development Team, 2023. QGIS Geographic Information System Software, Version 3.34.0-Prizren. Open Source Geospatial Foundation. qgis.org (3 March 2026).

Rad, A. M., Kreitler, J., & Sadegh, M., 2021: Augmented Normalized Difference Water Index for improved surface water monitoring. *Environmental Modelling & Software*, 140, 105030. doi.org/10.1016/j.envsoft.2021.105030.

Ronneberger, O., Fischer, P., & Brox, T., 2015: U-Net: Convolutional Networks for Biomedical Image Segmentation (arXiv:1505.04597). arXiv. doi.org/10.48550/arXiv.1505.04597.

Seale, C., Redfern, T., Chatfield, P., Luo, C., & Dempsey, K., 2022: Coastline detection in satellite imagery: A deep learning approach on new benchmark data. *Remote Sensing of Environment*, 278, 113044. doi.org/10.1016/j.rse.2022.113044.

ShoreZone, 2025. BC ShoreZone Map. Shorezone.Org. www.shorezone.org/shorezone-maps/bc-shorezone-map/ (31 March 2025).

Thomson, R. E., 1981: *Oceanography of the British Columbia coast*. Dept. of Fisheries and Oceans.

Vos, K., Harley, M. D., Splinter, K. D., Simmons, J. A., & Turner, I. L., 2019: Sub-annual to multi-decadal shoreline variability from publicly available satellite imagery. *Coastal Engineering*, 150, 160–174. doi.org/10.1016/j.coastaleng.2019.04.004.

Vos, K., Splinter, K. D., Harley, M. D., Simmons, J. A., & Turner, I. L., 2019: *CoastSat*: A Google Earth Engine-enabled Python toolkit to extract shorelines from publicly available satellite imagery. *Environmental Modelling & Software*, 122, 104528. doi.org/10.1016/j.envsoft.2019.104528.

Vos, K., Splinter, K. D., Palomar-Vázquez, J., Pardo-Pascual, J. E., Almonacid-Caballer, J., Cabezas-Rabadán, C., Kras, E. C., Luijendijk, A. P., Calkoen, F., Almeida, L. P., Pais, D., Klein, A. H. F., Mao, Y., Harris, D., Castelle, B., Buscombe, D., & Vitousek, S., 2023: Benchmarking satellite-derived shoreline mapping algorithms. *Communications Earth & Environment*, 4(1), 1–17. doi.org/10.1038/s43247-023-01001-2.

Wachmann, A., Mora-Soto, A., Yakimishyn, J., Bohlen, K., Fulton, E., & Costa, M., 2026: Centennial persistence of kelp forests on the West Coast of Vancouver Island, Canada. *Frontiers in Marine Science*, 13. doi.org/10.3389/fmars.2026.1720284.

Wang, R., Camilo, J., Collins, L. M., Bradbury, K., & Malof, J. M., 2017: The poor generalization of deep convolutional networks to aerial imagery from new geographic locations: An empirical study with solar array detection. *2017 IEEE Applied Imagery Pattern Recognition Workshop (AIPR)*, 1–8. doi.org/10.1109/AIPR.2017.8457965.

Xu, H., 2006: Modification of normalised difference water index (NDWI) to enhance open water features in remotely sensed imagery. *International Journal of Remote Sensing*, 27(14), 3025–3033. doi.org/10.1080/01431160600589179.

Yang, T., Jiang, S., Hong, Z., Zhang, Y., Han, Y., Zhou, R., Wang, J., Yang, S., Tong, X., & Kuc, T., 2020: Sea-Land Segmentation Using Deep Learning Techniques for Landsat-8 OLI Imagery. *Marine Geodesy*, 43(2), 105–133. doi.org/10.1080/01490419.2020.1713266.